J Solid State Electrochem (2010) 14:2057–2064
DOI 10.1007/s10008-010-1037-5

ORIGINAL PAPER

Electrochemical impedance spectroscopic studies of copper dissolution in glycine–hydrogen peroxide solutions

R. Prasanna Venkatesh · S. Ramanathan

Received: 30 November 2009 / Revised: 4 February 2010 / Accepted: 22 February 2010 / Published online: 19 March 2010

Abstract Anodic dissolution of copper in glycine solution at various hydrogen peroxide concentrations was investigated. The dissolution rate increases, reaches a maximum, and then decreases with hydrogen peroxide concentration. Anodic polarization studies and electrochemical impedance spectroscopy (EIS) studies were carried out to determine the mechanistic pathway of anodic dissolution of copper in glycine system at three different hydrogen peroxide concentrations: one at low hydrogen peroxide concentration in the active dissolution region, another in the maximum dissolution region, and the third at the high hydrogen peroxide concentration in the post-peak-dissolution region. The EIS data in complex plane plots show presence of two capacitance loops and one negative capacitance loop. The impedance plot patterns strongly depend on the hydrogen peroxide concentration in solution. Reaction mechanism analysis technique was employed to model the EIS data. A three-step mechanism with two intermediate adsorbates and a parallel dissolution by catalytic mechanism simulates EIS patterns which match the experimental trends. The intermediates are likely to be cupric and cuprous oxides. The essential features of impedance spectra at various overpotentials at three different hydrogen peroxide concentrations are captured by the proposed mechanism. The results also show that the film present on the copper surface in glycine and hydrogen peroxide solutions does not passivate the surface.

R. Prasanna Venkatesh · S. Ramanathan (✉)
Department of Chemical Engineering,
Indian Institute of Technology-Madras,
Chennai 600036, India
e-mail: srinivar@iitm.ac.in

Keywords Copper · Chemical mechanical polishing · Glycine · Hydrogen peroxide · Electrochemical impedance spectroscopy · Reaction mechanism analysis

Introduction

Anodic dissolution of copper in solutions is of importance in corrosion as well as chemical mechanical polishing (CMP). In the last decade, copper has replaced aluminum as interconnect material in semiconductor chips [1]. CMP of copper is a key process in fabrication of copper interconnects. Usually, slurry containing an oxidizing agent, a complexing agent, an inhibiting agent, and abrasive particles is used to remove excess copper in the CMP process [2, 3]. The excess copper is removed by the combined action of chemical dissolution and mechanical abrasion.

Slurries containing hydrogen peroxide as oxidizing agent and glycine as the complexing agent have been extensively studied [4-9]. The studies reveal that the copper removal rate increases with hydrogen peroxide concentration, reaches a maximum, and then decreases with further addition of hydrogen peroxide [7, 8]. This is explained as follows: at low concentrations, the hydrogen peroxide increases the copper oxidation rate, and hence, the dissolution rate increases. At higher concentrations, a copper oxide film is formed on the copper surface which inhibits further oxidation of copper, and hence, the polish rate decreases. However, anodic polarization curves of copper in glycine and hydrogen peroxide solutions do not show the usual sign of passivation [6, 7, 10]. The removal rate also does not go to zero at high hydrogen peroxide concentration [8]. Besides, at acidic pH range, copper oxides are not expected to be stable [11]. Even in alkaline pH range, addition of glycine decreases the stability region

of copper oxides [12]. The dissolution of copper in glycine and hydrogen peroxide solution has been studied by electrochemical impedance spectroscopy (EIS), in the frequency range of a few hertz to a few kilohertz [6]. A mechanism involving one faradaic reaction and six non-faradaic reactions was proposed to explain the dissolution. The model did not include a passivating oxide film and yet, could successfully explain the observed results [6]. Thus, while dissolution and CMP experiments show that the removal rates are low at high hydrogen peroxide concentrations, electrochemical experiments and potential–pH diagrams indicate that a passivating oxide may not form on the surface. A discontinuous oxide film may form on the surface, thereby retarding the dissolution and CMP, but not completely passivating the surface.

Various mechanisms have been proposed to explain the dissolution of copper in solutions. Copper electro-dissolution in 1 M sulfate medium was studied by EIS [13]. By comparing the EIS data and model characteristics, the following multi-step mechanism involving a catalytic reaction was proposed.

$$Cu \underset{k_{-1}}{\overset{k_1}{\rightleftharpoons}} Cu(I)_{ads} + e^-$$

$$Cu + Cu(I)_{ads} \xrightarrow{k_2} Cu^{2+}_{soln} + Cu(I)_{ads} + 2e^-$$

$$Cu(I)_{ads} \underset{k_{-3}}{\overset{k_3}{\rightleftharpoons}} Cu(II)_{ads} + e^-$$

$$Cu(II)_{ads} + Cu \xrightarrow{k_4} Cu^{2+}_{soln} + Cu(II)_{ads} + 2e^-$$

Another report presented the results of EIS experiments for copper dissolving in acidic sulfate medium at constant potential [14], and a multi-step mechanism involving a catalytic reaction was proposed to explain the data. The proposed mechanism is given below.

$$Cu \underset{k_{-1}}{\overset{k_1}{\rightleftharpoons}} Cu(I)_{ads}$$

$$Cu(I)_{ads} \underset{k_{-2}}{\overset{k_2}{\rightleftharpoons}} Cu(II)_{ads} + e^-$$

$$Cu(I)_{ads} \underset{k_{-3}}{\overset{k_3}{\rightleftharpoons}} Cu(I)^{*}_{ads} \xrightarrow{\text{diffusion}} Cu(I)_{sol}$$

$$Cu(II)_{ads} + Cu \xrightarrow{k_4} Cu(II)_{sol} + Cu(II)_{ads} + 2e^-$$

The EIS study of dissolution of copper in 1 M HCl at low current densities has been reported [15], and a two-step mechanism involving adsorbed cuprous chloride intermediate was proposed to explain most of the data exhibiting single or two capacitive loops

$$Cu_{ads} + Cl^- \underset{k_{-1}}{\overset{k_1}{\rightleftharpoons}} CuCl_{ads} + e^-$$

$$CuCl_{ads} + Cl^- \underset{k_{-2}}{\overset{k_2}{\rightleftharpoons}} CuCl_2$$

EIS data of copper dissolving in glycine and hydrogen peroxide solution were analyzed using an electrical equivalent circuit with three positive capacitances and three positive resistances [6]. The spectra at various potentials were acquired at a frequency of a few hertz and higher. A multi-step mechanism with one faradaic reaction and six non-faradaic reactions was proposed to explain the dissolution

$$2Cu + H_2O_2 \rightleftarrows Cu_2O + H_2O$$

$$Cu_2O + H_2O_2 \rightleftarrows 2CuO + H_2O$$

$$Cu_2O + H_2O \rightleftarrows 2CuO + 2H^+ + 2e^-$$

$$Cu + 2(^*OH) \rightleftarrows CuO + H_2O$$

$$CuO + {}^+H_3NCH_2COO^- + H^+ \rightleftarrows Cu(H_2NCH_2COO)^+ + H_2O$$

$$Cu(H_2NCH_2COO)^+ + H^+ \rightleftarrows Cu(H_3NCH_2COO)^{2+}$$

$$Cu(H_3NCH_2COO)^{2+} + {}^+H_3NCH_2COO^- \rightleftarrows Cu(H_2NCH_2COO)_2 + 2H^+$$

In the present work, we study the dissolution of copper in glycine–hydrogen peroxide system using EIS. The dissolution of copper at three different hydrogen peroxide concentrations was characterized using EIS, and the results were analyzed by employing reaction mechanism analysis (RMA). Various candidate mechanisms were used to fit the data, and we show that a three-step mechanism with two adsorbed intermediates, along with a parallel catalytic dissolution pathway explain the observed results. The intermediates are likely to be cuprous and cupric oxides.

Experimental

A conventional three-electrode electrochemical cell connected to the PARSTAT 2263 electrochemical instrument (Princeton Applied Research) was used to carry out all the electrochemical experiments. The working electrode was a copper rod of 9 mm diameter (99.9999% purity, Aldrich), whereas the reference and counter electrodes were Ag/AgCl (3.5 M KCl) and platinum electrode (both from CH instruments), respectively. The cell was placed inside a Faraday cage to minimize interference from electrical noise. Sodium sulfate (0.1 M) was used as supporting electrolyte in all electrochemical experiments to reduce the solution resistance. The solutions contained 1 wt.% glycine and various concentrations of hydrogen peroxide. All the chemicals are of analytical grade, and MilliQ (Millipore) water was used for all the experiments. Anodic polarization curves were obtained by scanning the potential at a rate of 1 mV/s. The impedance data were acquired by superimposing an AC perturbation of 10 mV in the frequency range of 100 kHz–200 mHz over the DC potential. Sequential quadratic programming was used to estimate the RMA parameters.

Dissolution experiments were carried out with electrochemical grade copper disk. The disk was initially polished

with fine sand paper, washed with dilute nitric acid solution to remove native oxide from the surface, dried in air stream, and weighed in a balance (Sartorius, BT 224S, 0.1 mg accuracy). Subsequently, it was immersed in the solution of interest for a period of 30 min. After 30 min, the copper disk was washed with MilliQ water and dried in zero air stream and weighed again. At least three identical runs were conducted, and the average dissolution rates along with the standard deviations are reported.

Results and discussion

Dissolution studies

Figure 1 shows the dissolution rate of copper in 1 wt.% glycine–0.1 M Na_2SO_4 solution as a function of hydrogen peroxide concentration. The dissolution rate increases with hydrogen peroxide concentration, reaches a maximum at 1% (*v*/*v*) hydrogen peroxide and then decreases. A similar trend has been reported for copper dissolving in solutions containing 0.01 M glycine and various hydrogen peroxide concentrations at a pH of 4 and 9 [8] and for copper dissolving in hydrogen peroxide and arginine, which is another amino acid [16]. Since the dissolution rate shows a maximum with respect to the hydrogen peroxide concentration, we chose to probe the dissolution mechanism at three regions with respect to the hydrogen peroxide concentration: one at 0.25% (*v*/*v*) hydrogen peroxide in the pre-peak region, another at 1% (*v*/*v*) hydrogen peroxide in the peak region, and the third one at 5% (*v*/*v*) hydrogen peroxide in the post-peak region. It must also be noted that, while the dissolution rate is relatively low at 5% (*v*/*v*) hydrogen peroxide, it is still higher than the dissolution rate in solution without hydrogen peroxide.

Electrochemical studies

The anodic polarization studies were carried out for copper dissolving in 1 wt.% glycine–0.1 M Na_2SO_4 solution at three different hydrogen peroxide concentrations, and the results are presented in Fig. 2. It is clear from the figure that there is no sign of passivation in all the three hydrogen peroxide concentrations in the scan range employed. Similar trends were reported for copper dissolving in 1 wt.% glycine and 5% (*v*/*v*) hydrogen peroxide solution with 0.1 M sodium nitrate as supporting electrolyte [6] and for copper dissolving in 0.1 M glycine with various hydrogen peroxide concentrations at pH 4, without any additional supporting electrolyte [7]. In order to determine the dissolution mechanism at all the three hydrogen peroxide concentrations, impedance studies were carried out at five anodic potentials for each concentration of hydrogen peroxide.

EIS is a versatile technique used to determine the kinetics of electrochemical reactions [15, 17-24]. The EIS data must be validated with Kramer–Kronig transformation (KKT) for casuality, stability, and linearity [19]. All the data reported here have been validated with KKT. Figure 3a shows the complex plane plot of EIS data for copper dissolving in 1 wt.% glycine, 0.1 M sodium sulfate-supporting electrolyte, and 0.25% (*v*/*v*) hydrogen peroxide. The diagram shows two capacitive loops separated by a pseudo-inductive arc. Since there are no magnetic fields associated with the dissolution process, and since the typical inductance values needed to model the data are very high, these loops are called as pseudo-inductive, or more appropriately, as negative capacitance arcs [23, 25]. The expanded view of the negative capacitance arc and low-frequency positive capacitance arc are shown in Fig. 3b for clarity. The capacitance at higher frequency would arise due to the double layer while the negative and positive capacitance loops at the low frequencies would arise from faradaic processes. The figure also shows that, as the potential increases, the overall impedance decreases, while the pattern remains the same.

Figure 3c, d show the complex plane plots of EIS data for copper dissolving in solutions containing 1 wt.% glycine and 0.1 M Na_2SO_4 with 1% (*v*) and 5% (*v*/*v*) hydrogen peroxide, respectively. The spectra show that there are two capacitive loops at the higher and middle frequency regime, while there is a negative capacitive loop

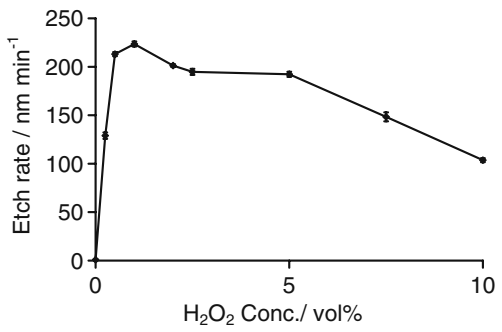

Fig. 1 Dissolution rate of copper in solutions containing 1wt.% glycine–0.1 M Na_2SO_4 at various hydrogen peroxide concentrations

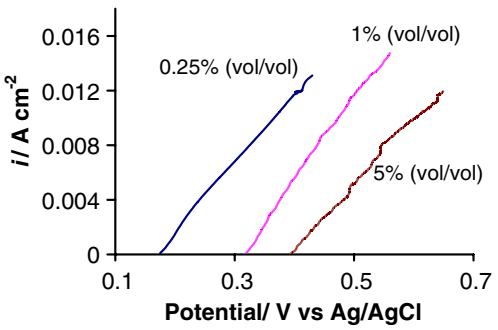

Fig. 2 (Color online) Anodic polarization curves of copper in solutions containing 1wt.% glycine–0.1 M Na_2SO_4 at various hydrogen peroxide concentrations

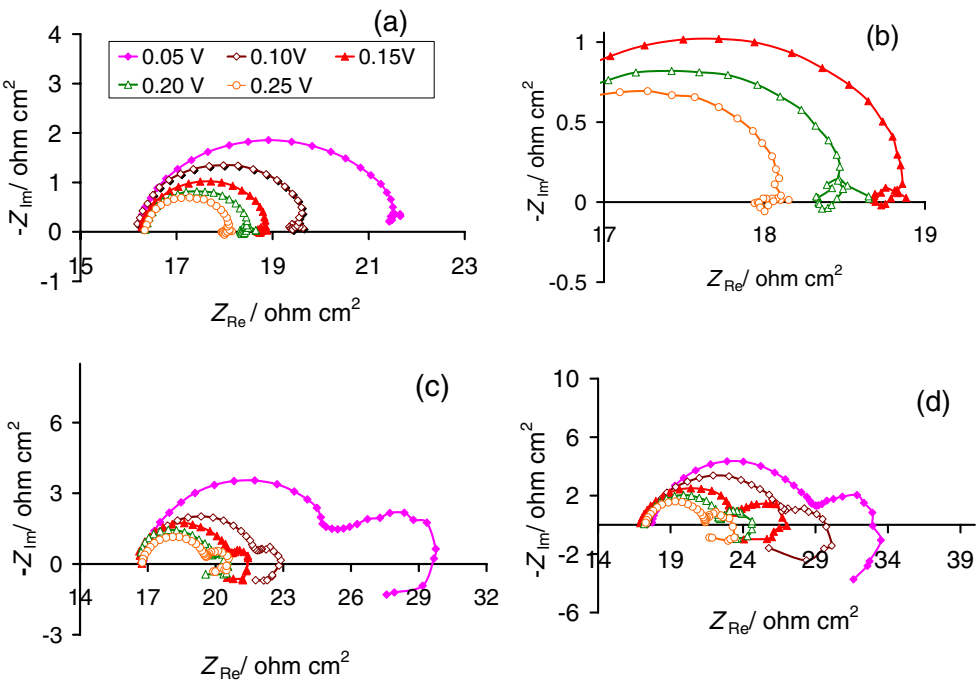

Fig. 3 (Color online) Experimental EIS data at various overpotentials for copper electrode in 1wt.% glycine–0.1 M Na_2SO_4 with **a** 0.25% (*v*/*v*) H_2O_2 **b** part of 0.25% (*v*/*v*) H_2O_2 enlarged **c** 1% (*v*/*v*) H_2O_2, and **d** 5% (*v*/*v*) H_2O_2. The *lines* are drawn for guiding the eye and do not represent any data fit

at the low-frequency regime. It must be noted that the negative capacitive loop is observed at intermediate frequencies for the 0.25% (*v*/*v*) hydrogen peroxide concentration and at low frequencies for 1% and 5% (*v*/*v*) hydrogen peroxide concentration. Also, for a given solution, an increase in overpotential causes a decrease in the overall impedance indicating that passivation does not occur at least in the regime investigated.

Reaction mechanism analysis

The EIS data show three time constants, viz., two capacitance loops and a negative capacitance loop for all the three solutions. Literature report [26] indicates that such patterns can arise from mechanisms with two adsorbed species. Our simulation results [27] also show that many other simpler mechanisms involving one adsorbed species would not produce such patterns and that at least two adsorbed species are necessary to simulate the patterns. Hence, simpler mechanisms such as direct dissolution or those with one intermediate species were excluded.

The details of derivation of impedance for various reactions have been presented in literature [28-30] and are summarized below for the proposed mechanism.Consider the following mechanism with two intermediates

$$\mathrm{Cu} \xrightarrow{k_1} \mathrm{Cu}^{+}_{\mathrm{ads}} + \mathrm{e}^{-} \tag{1}$$

$$\mathrm{Cu}^{+}_{\mathrm{ads}} \xrightarrow{k_2} \mathrm{Cu}^{2+}_{\mathrm{ads}} + \mathrm{e}^{-} \tag{2}$$

$$\mathrm{Cu}^{2+}_{\mathrm{ads}} \xrightarrow{k_3} \mathrm{Cu}^{2+}_{\mathrm{sol}} \tag{3}$$

The last step is the dissolution of the cupric species. It may also occur through the catalytic step, as given below.

$$\mathrm{Cu}^{2+}_{\mathrm{ads}} + \mathrm{Cu} \xrightarrow{k_4} \mathrm{Cu}^{2+}_{\mathrm{ads}} + \mathrm{Cu}^{2+}_{\mathrm{sol}} + 2\mathrm{e}^{-} \tag{4}$$

This is called as catalytic step since one of the species Cu^{2+}_{ads}involved in the reaction is regenerated. In this, the charged adsorbed species is associated with a kink or half-crystal atom on a dissolving edge of a terrace [17]. First, the anions present in the solution would be associated with the adsorbed species. Next, they would attach to the neighboring vacant site and allow the transfer of two electrons, thus transforming the vacant site to Cu^{2+}_{ads} species, while, simultaneously, the original adsorbed species will be dissolved into the solution. Thus, during this reaction, the charged adsorbed species is regenerated, and the active site for dissolution is transferred to the next atom of the dissolution edge. Hence, the catalytic step can be written in two steps as follows:

$$\mathrm{Cu}_1 + \mathrm{Cu}^{2+}_{2-\mathrm{ads}} \rightleftarrows \mathrm{Cu}_1 - \mathrm{Cu}^{2+}_{2-\mathrm{ads}} \tag{5}$$

$$\mathrm{Cu}_1 - \mathrm{Cu}^{2+}_{2-\mathrm{ads}} \rightarrow \mathrm{Cu}^{2+}_{1-\mathrm{ads}} + \mathrm{Cu}^{2+}_{2-\mathrm{sol}} + 2\mathrm{e}^{-} \tag{6}$$

In the above equations, the subscripts 1 and 2 are used to identify the individual atoms and to explicitly show the regeneration of the catalytic species.

In these equations, the *k*'s are the rate constants given by

$$k_i = k_{i0} \mathrm{e}^{b_i v} \tag{7}$$

where

$$b_{\mathrm{i}} = \pm \frac{\alpha_{\mathrm{i}} nF}{RT} \tag{8}$$

Here, α_i is the transfer coefficient with a value between 0 and 1, n is the number of electrons transferred in the step, F is the Faraday constant, R is the universal gas constant and T is the temperature in kelvin. For the case where $n>1$, it is simpler to assume that it is a single multi-electron transfer step, although it may be a sequence of one-electron processes. When the electron transfer is actually a sequence of one-electron processes, one of which is a rate determining step, the transfer coefficient of the overall reaction is given by $\alpha n = n_p + n_r \beta_m$ where n_p is the number of electrons transferred prior to the rate determining step, n_r is the number of electrons transferred after the rate determining step, and β_m is the modified symmetry factor of the actual rate determining step. The modified symmetry factor β_m is related to the symmetry factor β by the formula $\beta_m = \frac{2\beta+1}{4}$ [31]. In the present case, it is assumed that for the catalytic pathway, both electrons are transferred in a single step.

The unsteady state mass balance for the above mechanism can be written as follows.

$$\tau \frac{d\theta_1}{dt} = k_1(1-\theta_1-\theta_2) - k_2\theta_1 \tag{9}$$

$$\tau \frac{d\theta_2}{dt} = k_2\theta_1 - k_3\theta_2 \tag{10}$$

Where θ_1 and θ_2 are the surface coverages of the Cu^+ and Cu^{2+} species and τ is the number of surface sites per unit area. The steady-state surface coverages are given by

$$\theta_{1ss} = \frac{k_1 k_3}{k_1 k_2 + k_3 k_2 + k_3 k_1} \tag{11}$$

$$\theta_{2ss} = \frac{k_2}{k_3}\theta_{1ss} \tag{12}$$

The current density is given by

$$J = F[k_1(1-\theta_1-\theta_2)+k_2\theta_1)] + 2Fk_4\theta_2(1-\theta_1-\theta_2) \tag{13}$$

The first part corresponds to dissolution by the normal pathway, and the second part corresponds to the dissolution by catalytic pathway. The faradaic impedance $\left(Z_{F,m/s}\right)$ is obtained by taking the derivative of above equation with respect to the voltage and is given by

$$\left(Z_{F,m/s}\right)^{-1} = \frac{dJ}{dV} = (R_t)^{-1} - F[k_1 - k_2 + 2k_4\theta_{2ss}]\frac{d\theta_1}{dV} - F[k_1 + 2k_4\theta_{2ss} - 2k_4(1-\theta_{1ss}-\theta_{2ss})]\frac{d\theta_2}{dV} \tag{14}$$

where

$$(R_t)^{-1} = F[k_2\theta_{1ss}(b_1+b_2)] + 2F[\theta_{2ss}(1-\theta_{1ss}-\theta_{2ss})]k_4 b_4 \tag{15}$$

$$\frac{d\theta_1}{dV} = \frac{CE - BG}{AE - BD} \tag{16}$$

$$\frac{d\theta_2}{dV} = \frac{G - D\frac{d\theta_1}{dV}}{E} \tag{17}$$

where

$$A = k_1 + k_2 + j\omega\tau \tag{18}$$

$$B = k_1 \tag{19}$$

$$C = k_2\theta_{1ss}(b_1 - b_2) \tag{20}$$

$$D = -k_2 \tag{21}$$

$$E = k_3 + j\omega\tau \tag{22}$$

$$G = (b_2 - b_3)k_2\theta_{1ss} \tag{23}$$

R_t represents the resistance to charge transfer. The equation for total impedance is given below

$$Z_{Total} = R_{sol} + \frac{1}{Y_0(j\omega)^m + \left(Z_{F,m/s}\right)^{-1}} \tag{24}$$

Here Y_o represents the parameter of constant phase element (CPE), and m represents the exponent for CPE. Since the EIS data show a depressed semicircle in the high frequency regime, a constant phase element rather than a simple capacitor is used in the circuit to represent the double layer.

The RMA parameter set is obtained by minimizing the following error term

$$\text{error} = \sum [w_{Re}\left(Z_{Re_{experimental}} - Z_{Re_{bestfit}}\right)^2 + w_{Im}\left(Z_{Im_{experimental}} - Z_{Im_{bestfit}}\right)^2] \tag{25}$$

The error is taken over all the frequencies and over-potentials. Here w_{Re} and w_{Im} are the weighing functions which can be chosen as unity or as the inverse of value of real and imaginary parts [19]. If the impedance values span over an order of magnitude or more, the choice of weight may make a significant difference in optimized parameter set. However, in this case, the parameter values were not very sensitive to the weight function, and hence, unity weight function is used for RMA simulations. The data fit for all the three hydrogen peroxide concentrations is shown in Fig. 4a–d, and the RMA parameters are given in Table 1. Though there is a quantitative difference in impedance values between model and experimental data, the proposed mechanism captures the essential features observed in

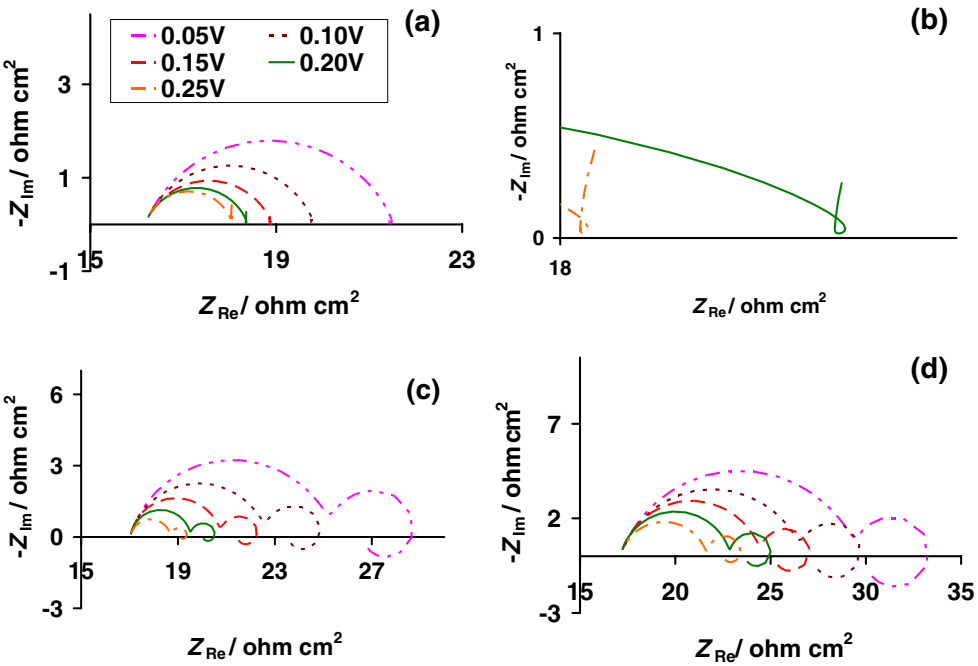

Fig. 4 (Color online) Best-fit RMA results at various overpotentials for copper in 1wt.% glycine–0.1 M Na_2SO_4 with **a** 0.25% (*v*/*v*) H_2O_2 **b** part of 0.25% (*v*/*v*) H_2O_2 enlarged **c** 1% (*v*/*v*) H_2O_2, and **d** 5% (*v*/*v*) H_2O_2

experiments at all hydrogen peroxide concentration. Elimination of catalytic reaction from the mechanism leads to more serious deviations between the simulated and experimental data.

Y_0 and m are not a strong function of overpotential for any of the three solutions. However, the value of m is lower for 0.25% (*v*/*v*) hydrogen peroxide, whereas for other higher hydrogen peroxide concentrations, the value ranges from 0.8–0.9. Similar non-ideal behavior for double layer has been reported in the literature for other systems [16, 32, 33]. The deviation of m from 1 is attributable to surface nonhomogeneities [34]. The nonhomogeneity may arise

Table 1 Best-fit parameters used for RMA

Parameter	Value for various H_2O_2 concentrations			Units
	0.25% (*v*/*v*)	1% (*v*/*v*)	5% (*v*/*v*)	
R_{sol}	16.2	17.0	17.1	Ohm cm^2
k_{10}	$3.92\ 10^{-6}$	$6.22\ 10^{-7}$	$9.86\ 10^{-12}$	Moles s^{-1} cm^{-2}
b_1	12.2	3.9	4.5	V^{-1}
k_{20}	$1.56\ 10^{-8}$	$9.86\ 10^{-8}$	$6.22\ 10^{-11}$	Moles s^{-1} cm^{-2}
b_2	2.4	5.1	0.9	V^{-1}
k_{30}	$1.56\ 10^{-8}$	$9.86\ 10^{-8}$	$6.22\ 10^{-11}$	Moles s^{-1} cm^{-2}
b_3	12.6	0	3.3	V^{-1}
k_{40}	$2.48\ 10^{-5}$	$6.22\ 10^{-7}$	$6.22\ 10^{-7}$	Moles s^{-1} cm^{-2}
b_4	21.2	10.3	5.5	V^{-1}
Y_o at 0.05 V	$3.30\ 10^{-4}$	$9.38\ 10^{-5}$	$8.38\ 10^{-5}$	Ohm^{-1} cm^{-2} S^n
m at 0.05 V	0.75	0.84	0.80	
Y_o at 0.10 V	$3.40\ 10^{-4}$	$9.91\ 10^{-5}$	$1.10\ 10^{-4}$	Ohm^{-1} cm^{-2} S^n
m at 0.10 V	0.77	0.86	0.81	
Y_o at 0.15 V	$3.90\ 10^{-4}$	$8.45\ 10^{-5}$	$7.32\ 10^{-5}$	Ohm^{-1} cm^{-2} S^n
m at 0.15 V	0.76	0.91	0.85	
Y_o at 0.20 V	$3.30\ 10^{-4}$	$6.20\ 10^{-5}$	$4.98\ 10^{-5}$	Ohm^{-1} cm^{-2} S^n
m at 0.20 V	0.78	0.94	0.87	
Y_o at 0.25 V	$2.50\ 10^{-4}$	$5.54\ 10^{-5}$	$5.38\ 10^{-5}$	Ohm^{-1} cm^{-2} S^n
m at 0.25 V	0.82	0.93	0.86	
τ	$6.22\ 10^{-7}$	$2.48\ 10^{-8}$	$7.83\ 10^{-12}$	Moles cm^{-2}

either from surface roughness or from the changes in chemical nature such as the presence of cupric or cuprous oxides. A value of 0.75 observed here indicates that both the surface roughness and chemical nonhomogeneities would contribute to the observed behavior. The data also indicates that the nonhomogeneities are comparable between the copper surface at 1% and 5% (*v*/*v*) hydrogen peroxide, while it is likely to be more for the copper surface in 0.25% (*v*/*v*) hydrogen peroxide. The Y_0 values do not show a strong dependence on the overpotential. The value of *m* increases with overpotential indicating that perhaps the nonhomogeneities are reduced due to more dissolution.

The surface coverage of both adsorbed species Cu^+ and Cu^{2+} for all the three hydrogen peroxide concentrations are given in Fig. 5a, b. The species are likely to be cuprous and cupric oxides. While the potential–pH diagrams predict that they will not be stable at the acidic pH, the dynamic nature of the process may allow for a sub-monolayer thin film formation on the surface. For solution containing 0.25% (*v*/*v*) H_2O_2, the surface coverage of Cu^+ is more than 0.6 at overpotential of 50 mV, and it increases with overpotential. While each one of the rate constant increases with the overpotential, the steady-state surface coverage values are determined by the ratio of the rate constants as given by the Eqs. 11 and 12. The surface coverage of Cu^{2+} decreases with overpotential, and there is very little vacant copper site. The reaction rate of dissolution of Cu^{2+} by normal kinetics (Eq. 3) is relatively lower than the rate of dissolution through catalytic step (Eq. 4). The catalytic step requires that the Cu^{2+} and a vacant site be adjacent to each other. Although the fraction of vacant copper sites is low for copper dissolving in 0.25% (*v*/*v*) H_2O_2, the rate constant k_4 is three orders of magnitude higher than the rate constant k_3 and hence almost 80% of the copper dissolution occurs by catalytic step while the remaining 20% occurs by non-catalytic pathway at all the overpotentials.

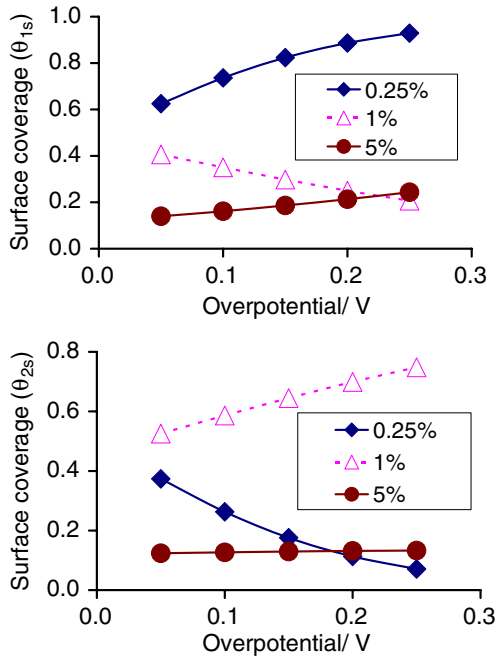

Fig. 5 (Color online) Variation of cuprous and cupric species surface coverage with over potential at three different hydrogen peroxide concentrations of 0.25% (*v*/*v*), 1% (*v*/*v*), and 5% (*v*/*v*)

In case of 1% (*v*/*v*) H_2O_2 solution, the surface coverage of Cu^{2+} is more than that of Cu^+. Here, the surface coverage of Cu^{2+} increases with overpotential, while that of Cu^+ decreases with overpotential. The fractional surface coverage of vacant sites is in the range of 0.05 for this solution. The number of active sites (τ) is also an order of magnitude lower than those in 0.25% (*v*/*v*) H_2O_2 solution. This indicates that the surface may possibly be covered by a discontinuous film. Since the potential–pH diagrams indicate that a stable oxide would not form at acidic pH range, presence of a thick oxide film is less likely. Another possibility is that a large number of OH radicals may adsorb on the copper surface and block it. While the nature of the species that blocks the electrode is not clear, the fact that the number of active sites in the model is low indicates that most of the area is blocked. The dissolution by catalytic pathway is about 40% of the total dissolution at 50 mV overpotential. However, at 250 mV overpotential, almost 80% of the dissolution occurs by catalytic pathway, while the remaining 20% is by the non-catalytic dissolution.

In 5% (*v*/*v*) H_2O_2 solutions, the number of available sites (τ) is five orders of magnitude lower than those at 0.25% (*v*/*v*) H_2O_2 solutions. This indicates that most of the surface is blocked and that only an extremely small percent of the sites is available for dissolution. Here, the surface coverage of Cu^{2+} remains a constant at about 0.13 for all overpotentials, while the surface coverage of Cu^+ increases from 0.14 to 0.24 when the overpotential is increased from 50 to 250 mV. Correspondingly, the vacant site surface coverage decreases from 0.74 to 0.62. More than 99.99% of the dissolution occurs through the catalytic pathway, and the non-catalytic pathway can be neglected for all practical purposes. Presence of vacant site, even in very small quantities, facilitates dissolution by catalytic step, and hence, complete passivation does not occur.

Conclusions

The dissolution of copper in 1 wt.% glycine solution at various hydrogen peroxide concentrations was investigated. The dissolution rate exhibits a maximum at 1% (*v*/*v*) hydrogen peroxide. While the dissolution rate at higher hydrogen peroxide concentration is lower than the peak dissolution rate observed at 1% (*v*/*v*) H_2O_2, it is not very low. Anodic polarization data also do not show any kink for all the hydrogen peroxide concentrations. EIS data shows

two capacitance loops and a negative capacitance loop. The EIS pattern strongly depends on the hydrogen peroxide concentration. EIS data was analyzed using RMA to determine the kinetics. A three-step mechanism with cuprous and cupric oxide intermediates and a parallel catalytic dissolution models the observed data. The number of active dissolution sites decreases with increase in hydrogen peroxide concentrations. However, even when most of the copper is blocked and the number of active sites are low, the dissolution by catalytic pathway is significant and hence complete passivation does not occur.

Acknowledgement We would like to thank Prof. D.D. Macdonald (ddm@psu.edu) for providing the KKT software.

References

1. Steigerwald JM, Murarka SP, Gutmann RJ, Duquette DJ (1995) Mater Chem Phys 41:217
2. Steigerwald JM, Murarka SP, Gutmann RJ (1997) Chemical mechanical planarization of microelectronic materials. Wiley, New York
3. Oliver MR (2004) In: Oliver MR (ed) Chemical-mechanical planarization of semiconductor materials. Springer, Berlin
4. Li Y, Hariharaputhiran M, Babu SV (2001) J Mater Res 16:1066
5. Zeidler D, Stavreva Z, Plotner M, Drescher K (1997) Microelectron Eng 33:259
6. Lu J, Garland JE, Pettit CM, Babu SV, Roy D (2004) J Electrochem Soc 151(10):G717
7. Seal S, Kuiry SC, Heinmen B (2003) Thin Solid Films 423:243
8. Aksu S, Wang L, Doyle FM (2003) J Electrochem Soc 150(11):G718
9. Du T, Vijayakumar A, Desai V (2004) Electrochim Acta 49:4505
10. Ein-Eli Y, Abelev E, Rabkin E, Starosvetsky D (2003) J Electrochem Soc 150(9):C646
11. Pourbaix M (1974) Atlas of electrochemical equilibria in aqueous solutions, 2nd edn. NACE, Houston
12. Tamilmani S, Huang W, Raghavan S, Small R (2002) J Electrochem Soc 149(12):G638
13. Cordeiro GGO, Barcia OE, Mattos OR (1993) Electrochim Acta 38:319
14. Wong DKY, Coller BAW, Macfarlane DR (1993) Electrochim Acta 38(14):2121
15. Diard JP, Le Canut JM, Le Gorrec B, Montella C (1998) Electrochim Acta 43:2485
16. Nagendra Prasad Y, Vinod kumar V, Ramanathan S (2009) J Solid State Electrochem 13:1351
17. Keddam M (2002) In: Marcus P (ed) Corrosion mechanism in theory and practise. Dekker, New York
18. Macdonald JR (1990) Electrochim Acta 35:483
19. Macdonald JR (2005) In: Barsoukov E, Macdonald JR (eds) Impedance spectroscopy, 2nd edn. Wiley, NJ
20. Macdonald DD (2006) Electrochim Acta 51:1376
21. Diard JP, Le Gorrec B, Montella C (1992) J Electronal Chem 326:13
22. Diard JP, Le Gorrec B, Montella C (1993) J Electronal Chem 352:1
23. Harrington DA, van den Driessche P (2004) J Electronal Chem 567:153
24. Gregori J, Gimenez-Romero D, Garcia-Jareno JJ, Vicente F (2005) J Solid State Electrochem 9:83
25. Franceschetti DR, Macdonald JR (1977) J Electroanal Chem 82:271
26. Diard JP, LeGorrec B, Montella C, Montero-Ocampo C (1992) Electrochim Acta 37(1):177
27. Maddala J, Krishnaraj S, Vinod Kumar V, Ramanathan S (2010) J Electroanal Chem 638:183
28. Keddam M, Mattos OR, Takenouti H (1981) J Electrochem Soc 128:257
29. Macdonald DD, Real S, Smedley SI, Urquidi-Macdonald M (1988) J Electrochem Soc 135:2410
30. Bojinov M (1996) J ElectroanalChem 405:15
31. Fletcher S (2009) J Solid State Electrochem 13:537
32. Sadkowski A (2000) J Electroanal Chem 481:222
33. Sadkowski A (2000) J Electroanal Chem 481:232
34. Pajkossy T (2005) Solid State Ion 176:1997